THE JOURNAL OF BIOLOGICAL CHEMISTRY VOL. 286, NO. 40, pp. 35209–35217, October 7, 2011

Elucidation of the Molecular Basis of Selective Recognition Uncovers the Interaction Site for the Core Domain of Scorpion α-Toxins on Sodium Channels*[S]

Received for publication, May 10, 2011, and in revised form, August 5, 2011 Published, JBC Papers in Press, August 8, 2011, DOI 10.1074/jbc.M111.259507

Maya Gur[‡1], Roy Kahn[‡1], Izhar Karbat[‡], Noa Regev[‡], Jinti Wang[§], William A. Catterall[§2], Dalia Gordon[‡], and Michael Gurevitz[‡]

From the [‡]Department of Plant Molecular Biology and Ecology, George S. Wise Faculty of Life Sciences, Tel-Aviv University, Ramat-Aviv, Tel-Aviv 69978, Israel and the [§]Department of Pharmacology, School of Medicine, University of Washington, Seattle, Washington 98195-7280

Neurotoxin receptor site-3 at voltage-gated Na^+ channels is recognized by various peptide toxin inhibitors of channel inactivation. Despite extensive studies of the effects of these toxins, their mode of interaction with the channel remained to be described at the molecular level. To identify channel constituents that interact with the toxins, we exploited the opposing preferences of LqhαIT and Lqh2 scorpion α-toxins for insect and mammalian brain Na^+ channels. Construction of the DIV/S1-S2, DIV/S3-S4, DI/S5-SS1, and DI/SS2-S6 external loops of the rat brain $rNa_v1.2a$ channel (highly sensitive to Lqh2) in the background of the *Drosophila* $DmNa_v1$ channel (highly sensitive to LqhαIT), and examination of toxin activity on the channel chimera expressed in *Xenopus* oocytes revealed a substantial decrease in LqhαIT effect, whereas Lqh2 was as effective as at $rNa_v1.2a$. Further substitutions of individual loops and specific residues followed by examination of gain or loss in Lqh2 and LqhαIT activities highlighted the importance of DI/S5-S6 (pore module) and the C-terminal region of DIV/S3 (gating module) of $rNa_v1.2a$ for Lqh2 action and selectivity. In contrast, a single substitution of Glu-1613 to Asp at DIV/S3-S4 converted $rNa_v1.2a$ to high sensitivity toward LqhαIT. Comparison of depolarization-driven dissociation of Lqh2 and mutant derivatives off their binding site at $rNa_v1.2a$ mutant channels has suggested that the toxin core domain interacts with the gating module of DIV. These results constitute the first step in better understanding of the way scorpion α-toxins interact with voltage-gated Na^+-channels at the molecular level.

Voltage-gated sodium channels (Na_v)[3] play a central role in excitability (1) and are targeted by a large variety of toxins used for prey and defense (2). Among a number of binding sites (3), neurotoxin receptor site-3 has been defined pharmacologically as the channel site of interaction with peptide toxins from scorpions, sea anemones, and spiders capable of inhibiting the channel inactivation process. Despite their similar effect and ability to compete for binding (3–5), these toxins differ tremendously in structure (6, 7), thus raising questions as to commonalities and differences in the molecular structure of receptor site-3.

Na_vs are composed of a pore-forming α-subunit (~260 kDa) that in mammals is associated with one or two β-subunits and in insects with the TipE accessory subunit (1, 8–12). The α-subunit consists of four homologous domains (DI-DIV), each composed of six transmembrane segments (S1–S6) connected by intra- and extracellular loops. A key feature of Na_vs is the voltage-dependent activation enabled by the gating module formed by transmembrane segments S1–S4 in each of the four domains. The positively-charged S4 segments respond to changes in membrane potential and move outwards across the membrane electric field, leading to opening of the channel pore and transient increase in sodium conductance that is followed by fast inactivation (1, 13). The fast inactivation is coupled to the movement of the voltage sensor in DIV, which triggers the occlusion of the inner side of the channel pore by the intracellular loop that connects DIII and DIV (inactivation loop; 5, 14–16). Site-3 toxins have been shown to impede the movement of the voltage sensor in DIV, thereby inhibiting fast inactivation (17, 18).

Receptor site-3 has been localized at low resolution to the extracellular loops in domains I and IV using a photoaffinity-labeled scorpion α-toxin (Lqq5 from *Leiurus quinquestriatus quinquestriatus*) and antibodies directed to specific regions of the external loops in domains I (S5–S6) and IV (S3–S4 and S5–S6) of the rat brain channel $rNa_v1.2$ (19, 20). Channel chimeras between $rNa_v1.2$ and the cardiac channel subtype $rNa_v1.5$ (21, 22) suggested a role for DIV/S3-S4 loop in the interaction of $rNa_v1.2a$ brain channel with Lqq5. Of particular interest was the result of charge inversion at position 1613 (E1613R), which decreased the affinity for Lqq5 by 62-fold (21). Mutagenesis of nearby residues in the $rNa_v1.2a$ channel and the equivalent loop of the skeletal muscle Na_v ($rNa_v1.4$) suggested a putative role for other residues of DIV/S3-S4 (Asp-1428, Lys-1432, Tyr-1433, Phe-1434, and Val-1435) in the interaction of the sodium channel with scorpion α-toxins (21, 23, 24; Fig. 1).

* This work was supported, in whole or in part, by National Institutes of Health Grant 1U01 NS058039-01 (to W. A. C. and M. G.). This work was also supported by United States-Israel Binational Agricultural Research and Development Grant IS-4313-10 (to M. G. and D. G.) and by Israeli Science Foundation Grant 107/08 (to M. G. and D. G.).

[S] The on-line version of this article (available at http://www.jbc.org) contains supplemental Table 1 and Fig. 1.

[1] Both authors contributed equally to this work.

[2] To whom correspondence should be addressed: Dept. of Pharmacology, School of Medicine, University of Washington, Seattle, WA 98195-7280.

[3] The abbreviation used is: Na_v(s), voltage-gated sodium channel(s).

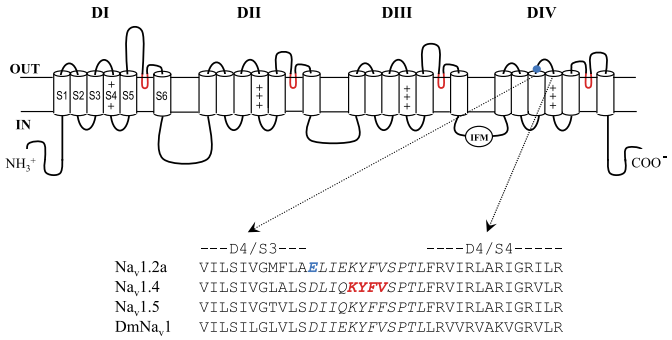

FIGURE 1. **Sodium channel topology.** *Top*, transmembrane folding diagram of the α-subunit of a voltage-gated sodium channel. *Cylinders* represent transmembrane α-helical segments. The gating module (segments S1–S4) of each domain resides near the pore module region (segments S5–S6) of the next domain in a clockwise orientation. *Boldface lines* represent the external and internal loops that connect the transmembrane segments. The pore loop (SS1–SS2) is colored *red*, and the inactivation ball is indicated by the IFM motif. Site-3 has been thus far assigned to the extracellular loops S5–S6 of DI and DIV and DIV/S3-S4 (19–21, 23, 24). The position of Glu-1613 is highlighted by a *blue circle*. *Bottom*, sequence alignment of DIV/S3-S4 extracellular loop (in *italics*) of the mammalian brain channel ($rNa_v1.2a$), mammalian skeletal muscle channel ($rNa_v1.4$), heart channel ($hNa_v1.5$) and *Drosophila* channel ($DmNa_v1$). Residue substitutions that affected the activity of scorpion α-toxins are in blue (Glu-1613 at $rNa_v1.2a$ DIV/S3-S4 (21)) and in *red* (Lys-1432, Tyr-1433, Phe-1434, and Val-1435 of $rNa_v1.4$ (23, 24)).

Despite these results, the channel components that constitute receptor site-3 have not been fully determined.

Scorpion α-toxins constitute a family of structurally related polypeptides of 61–67 amino acids reticulated by four conserved disulfide bridges. Despite the similarity in sequence and three-dimensional structure, these toxins exhibit substantial differences in preference for mammalian and insect Na_vs, and on this basis are subdivided into subgroups (reviewed in Ref. 3) (i) α-toxins highly active on mammals and very weak on insects, such as Aah2 from *Androctonus australis hector*, Lqh2 from *Leiurus quinquestriatus hebraeus* (EC_{50} = 13.6 ± 1.4 nM and 6920 ± 1420 nM on $rNa_v1.2a$ and the *Drosophila* $DmNa_v1$ channel, respectively, expressed in *Xenopus* oocytes; Ref. 25), and Lqq5 from *L. quinquestriatus quinquestriatus* (K_D = 1.71 ± 1.1 nM, as determined on $rNa_v1.2a$ expressed in tsA-201 cells; Ref. 21); (ii) α-toxins that are highly active on insects and very weak at mammalian brain Na_vs, such as LqhαIT (EC_{50} = 0.36 ± 0.04 nM on $DmNa_v1$, and 17800 ± 357 nM on $rNa_v1.2a$; Ref. 25); and (iii) α-like toxins that are active both in mammalian brain and on insects.

The pharmacology, electrophysiological effects, structures, and bioactive surfaces (see Fig. 2) of scorpion α-toxins have been studied extensively (3). Their functional surface is bipartite and is divided between two domains: a core domain that involves short loops that connect the conserved secondary structure elements of the molecule core and an NC domain composed of the five-residue turn (residues 8–12) and the C-terminal segment (see Fig. 2*A*; Refs. 26–29). The difference in amino acid composition and spatial arrangement of the NC domain was suggested to dictate the variations in preference among α-toxins for distinct Na_vs.

Here, we used two α-toxins, Lqh2 and LqhαIT, which vary greatly in preference for insect and mammalian brain Na_v, to analyze channel constituents involved in this selective recognition. We chose $Na_v1.2$ for construction of chimeric Na_v channels because it is more sensitive to Lqh2 and much less sensitive to LqhαIT than cardiac or skeletal muscle Na_V channels. Construction of $rNa_v1.2a$ external loops in the background of $DmNa_v1$ as well as point mutagenesis revealed the role of DI/S5-S6 and DIV/S3 in the selective recognition by Lqh2. Comparison of depolarization-induced dissociation of Lqh2 and its mutant derivatives from various channel mutants suggested that the core domain of Lqh2 interacts with the voltage-sensing module in DIV of the channel.

EXPERIMENTAL PROCEDURES

Toxin Production and Modification—Lqh2 was produced in *Escherichia coli* strain BL21 as described (29). The toxin derivatives bear a His_6 tag and a thrombin cleavage site at their N termini that does not hamper their activity (25).

Channel Modification—The cDNA encoding the $DmNa_v1$ sodium channel of *Drosophila melanogaster* cloned in pAlter expression vector (Promega) was digested by XbaI, ApaI, and NotI, dividing the entire sequence to two fragments, one encoding domains I and II (3650 bp) and the other encoding domains III and IV (2890 bp). The two fragments were cloned into pBluescript (Stratagene), and the resulting plasmids were used in all further steps of PCR-driven mutagenesis and construction of channel mutants. Mutagenized DNA fragments were back inserted to the original plasmid and the DNA sequence was verified prior to RNA production for injection into *Xenopus laevis* oocytes. The cDNA encoding the $rNa_v1.2a$ rat brain sodium channel, cloned in the expression vector pCDM8 (Invitrogen), was used in a similar way for mutagenesis, and BstEII and BspMI restriction sites were used for back insertion to the original plasmid.

Expression of Na_vs in Oocytes and Two-electrode Voltage Clamp Experiments—cRNAs encoding the α-subunit of each channel and the auxiliary β1 and TipE subunits were transcribed *in vitro* using T7 RNA polymerase and the mMESSAGE mMACHINE™ system (Ambion, Austin, TX) and injected into *Xenopus* oocytes as described previously (30). Currents were measured 1–3 days after injection using a two-electrode voltage clamp and a Gene Clamp 500 amplifier (Axon Instruments, Union City, CA). Data were sampled at 10 kHz and filtered at 5 kHz. Data acquisition was controlled by a Macintosh PPC 7100/80 computer, equipped with an ITC-16 analog/digital converter (Instrutech Corp., Port Washington, NY), utilizing Synapse (Synergistic Systems). Capacitance transients and leak currents were removed by subtracting a scaled control trace utilizing a P/6 protocol (31). Bath solution contained the following: 96 mM NaCl, 2 mM KCl, 1 mM $MgCl_2$, 1.8 mM $CaCl_2$, 5 mM HEPES, pH 7.5. Toxins were diluted with bath solution containing 1 mg/ml bovine serum albumin and applied directly to the bath in the final desired concentration. To avoid application artifacts, 1 mg/ml bovine serum albumin solution was applied prior to toxin addition. For the *G-V* analysis, mean conductance (G) was calculated from the peak current-voltage relations using the equation $G = I/(V - V_{rev})$, where I is the peak current, V is the membrane potential, and V_{rev} is the reversal potential. The normalized conductance-voltage relations were fit with either a one- or two-component Boltzmann distribution according to Equation 1,

$$G/G_{max} = (1 - A)/(1 + \exp[(V1_{1/2} - V)/k_1]) + A/(1 + \exp[(V2_{1/2} - V)/k_2]) \quad \text{(Eq. 1)}$$

where $V1_{½}$ and $V2_{½}$ are the respective membrane potentials for two populations of channels for which the mean conductance is half maximal, k_1 and k_2 are their respective slopes, and A defines the proportion of the second population (amplitude) with respect to the total. For fits in which only one population of channels was apparent, A was set to zero. The voltage dependence of steady-state fast inactivation was described using a single Boltzmann distribution as shown in Equation 2,

$$I/I_{max} = \alpha_0 + \alpha_1/(1 + \exp[(V - V_h)/k]) \quad \text{(Eq. 2)}$$

where I is the peak current obtained at the depolarizing test step, I_{max} is the current without a preceding conditioning step, V is the membrane potential of the conditioning step, V_h is the membrane potential at which half-maximal inactivation is achieved, k is the slope factor, α_0 is the remaining normalized peak current at highly depolarizing conditioning potentials, and α_1 is the normalized amplitude (32).

Dose-response Curves of α-Toxin Effect on Fast Inactivation—Currents were elicited by a 50-ms depolarization to −20 mV from a −80 mV holding potential in the presence of increasing toxin concentrations. At each toxin concentration, the currents were allowed to reach a steady-state level prior to the final measurement. The dose dependence for toxin-induced removal of fast inactivation is calculated by plotting the ratio of the steady-state current remaining 50 ms after depolarization (I_{ss}) to the peak current (I_{peak}) as a function of toxin concentration, normalized to the maximal effect set to 1, and fitted with the Hill equation, where H is the Hill coefficient, [toxin] is the toxin concentration, and a_0 is the offset measured prior to toxin application. The $a_1 - a_0$ amplitude provides the maximal effect obtained at saturating toxin concentrations. EC_{50} is the toxin concentration at which half-maximal inhibition of fast inactivation is obtained. To reduce variability, H was set to 1 in all calculations.

$$\frac{I_{ss}}{I_{peak}} = a_0 + \frac{a_1 - a_0}{1 + \left(\frac{EC_{50}}{[toxin]}\right)^H} \quad \text{(Eq. 3)}$$

Determination of Voltage-dependent Dissociation of Toxin—Voltage-dependent toxin dissociation was measured with a two-pulse protocol. Conditioning dissociation pulses between −20 mV to +105 mV were applied from a −100 mV holding potential, following 50 ms at −100 mV for channels recovery from fast inactivation. Sodium currents were then elicited with a 50-ms test pulse to −20 mV. The experiments were conducted at saturating toxin concentrations, and a 30-s interval between test pulses ascertained maximal toxin rebinding. The extent of removal of fast inactivation represented by the ratio I_{ss}/I_{peak} was plotted as a function of the conditioning voltage and was fitted with the Boltzmann distribution described in Equation 4,

$$I(V) = \frac{1}{1 + e^{\frac{V - V_{1/2}}{k_{1/2}}}} \quad \text{(Eq. 4)}$$

where $V_{½}$ is the half-maximal dissociation voltage, and $k_{½}$ is the corresponding slope factor.

RESULTS

The extreme difference in potency of Lqh2 and LqhαIT on $rNa_v1.2a$ rat brain and $DmNa_v1$ *Drosophila* voltage-gated sodium channels is correlated with differences in their bioactive surfaces as well as differences in their channel receptor sites. Whereas the toxins have been thoroughly dissected and their bioactive surfaces documented (Fig. 2) (26, 29), their channel receptor sites are described incompletely. Based on previous reports suggesting that receptor site-3 is associated with channel external loops of domains IV and I (19, 21, 23, 24, 33), our approach to identify channel constituents that determine toxin recognition was to first uncover the extracellular loops involved with toxin selectivity and then use this information to characterize toxin interaction with receptor site-3.

Construction of $rNa_v1.2a$ External Loops in $DmNa_v1$ and Analysis of Sensitivity to Lqh2 and LqhαIT—Stepwise construction of the four external loops DIV/S1-S2, DIV/S3-S4, DI/S5-SS1, and DI/SS2-S6 from $rNa_v1.2a$ in the background of $DmNa_v1$ (see sequences in supplemental Fig. 1) provided channel chimeras, which we named by indicating the parent channel in full type and the substituted segments or amino acid residues as superscripts (supplemental Table 1). The voltage-dependent activation and inactivation properties of these chimeras varied only slightly from those of $DmNa_v1$ (supplemental Table 1). However, the sensitivity of these chimeric channels to the two toxins varied greatly (Table 1). Most dramatic was the decrease in sensitivity of the final chimera $DmNa_v1^{rNav1.2a(DI/S5\text{-}SS1+SS2\text{-}S6,DIV/S1\text{-}S2+S3\text{-}S4)}$ to LqhαIT by nearly 3 orders of magnitude from an EC_{50} of 0.36 ± 0.04 nM for $DmNa_v1$ to an EC_{50} of 241 ± 47 nM for the chimera (Table 1). On the other hand, Lqh2 activity increased from an EC_{50} value of 6920 ± 1420 nM for $DmNa_v1$ to an EC_{50} value of 26.7 ± 3.1 nM for the chimera (Table 1 and Fig. 3*A*). This suggested that the mammalian receptor site-3 of Lqh2 has been nearly fully constructed in the background of the insect channel. Therefore, this chimera was named $DmNa_v1^{rNav1.2a(site\text{-}3\ face)}$.

To clarify the contribution of each loop to toxin recognition, we first examined the S1–S2 and S3–S4 external loops of the gating-module in DIV. Because $DmNa_v1^{rNav1.2a(DIV/S3\text{-}S4)}$ did not express in oocytes, we examined the sensitivity of $DmNa_v1^{rNav1.2a(DIV/S1\text{-}S2)}$ and $DmNa_v1^{rNav1.2a(DIV/S1\text{-}S2+S3\text{-}S4)}$ to Lqh2 and LqhαIT. The activity of Lqh2 on $DmNa_v1^{rNav1.2a(DIV/S1\text{-}S2+S3\text{-}S4)}$ was 58-fold higher compared with its activity on the unmodified $DmNa_v1$ and 4.5-fold weaker than that at $DmNa_v1^{rNav1.2a(Site\text{-}3\ face)}$, whereas the activity of LqhαIT on this chimera decreased 159-fold (Table 1). The swap of DIV/S1-S2 (chimera $DmNa_v1^{rNav1.2a(DIV/S1\text{-}S2)}$) improved Lqh2 activity by only 4.5-fold (Table 1), highlighting the greater significance of loop DIV/S3-S4 in determining the specificity of Lqh2 binding.

We next analyzed the external loops of DI pore module. The sensitivity of $DmNa_v1^{rNav1.2(DI/S5\text{-}SS1+SS2\text{-}S6)}$ to Lqh2 increased 56-fold compared with the sensitivity of $DmNa_v1$ to this toxin, whereas these substitutions had barely an effect on LqhαIT activity. However, the sensitivity of $DmNa_v1^{rNav1.2(DI/S5\text{-}SS1)}$

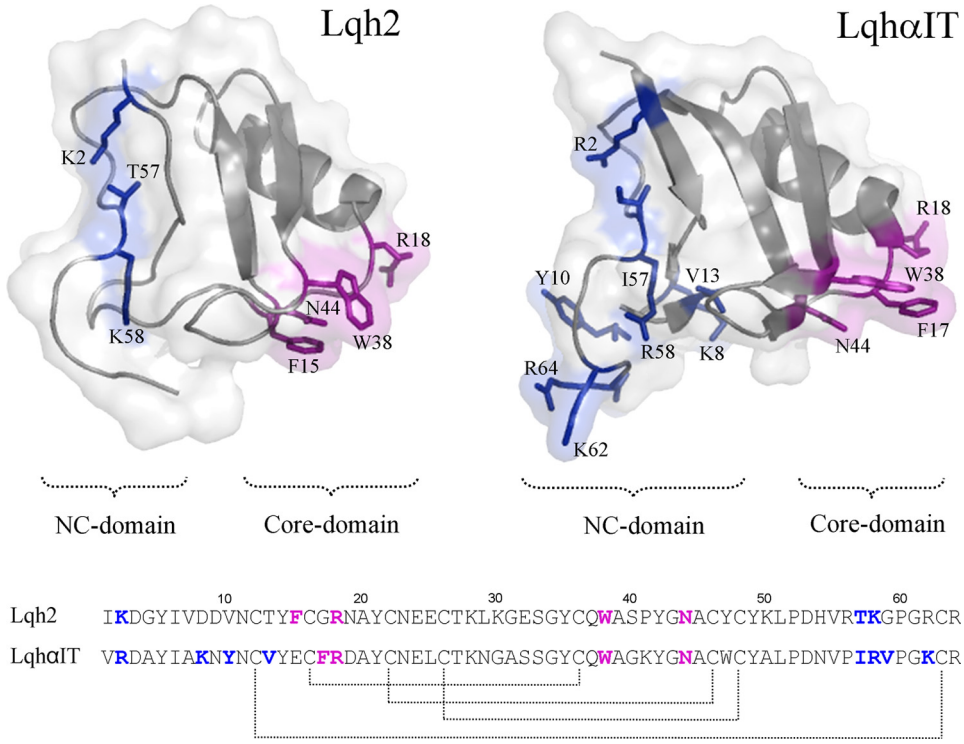

FIGURE 2. **Comparison of Lqh2 and LqhαIT.** *Top*, bioactive surfaces of the two toxins. Lqh2 modeling was based on the reported structure of the almost identical toxin Aah2 (Protein Data Bank code 1AHO), and LqhαIT structure was determined (Protein Data Bank code 2ASC). The *gray ribbons* indicate the backbone structures covered by a semitransparent molecular surface of the toxins. Bioactive residues are shown as sticks (26, 29, 40). Residues of the core domain are colored *magenta*, and residues of the NC domain are colored *blue*. *Bottom*, sequence alignment of the two toxins. The bioactive surface of scorpion α-toxins consists of the conserved core domain (residues in *magenta*) and the diverse NC domain (residues in *blue*). Lqh2 and LqhαIT are similar in structure and share ~70% sequence similarity, yet they exhibit opposing preferences for the mammalian brain and insect Na_vs (Table 1).

TABLE 1

Effect of Lqh2 and LqhαIT on channel mutants

The channels were clamped at a holding potential of −80 mV, and currents were elicited by depolarization to −20 mV in the presence of increasing toxin concentrations. At each toxin concentration, the currents were allowed to reach a steady-state level prior to the final measurement. Determination of dose-dependent effect of the toxin (removal of fast inactivation) is described in detail under "Experimental Procedures", and the EC_{50} values provided are mean ± S.E., where *n* stands for the number of cells analyzed. No effect denotes lack of effect on channel inactivation in the presence of 5 μM toxin.

Channel derivative	EC_{50} of Lqh2	EC_{50} of LqhαIT
	nM	nM
$DmNa_v1$ unmodified	6920 ± 1420	0.36 ± 0.04
$DmNa_v1^{D1701E}$	>5000 (n = 3)	50 ± 4.1 (n = 3)
$DmNa_v1^{D1701R}$	No effect	No effect
$DmNa_v1^{rNav1.2a(DIV/S1-S2)}$	1530 ± 433 (n = 4)	3.2 ± 0.6 (n = 5)
$DmNa_v1^{rNav1.2a(DIV/S1-S2+S3-S4)}$	120 ± 12 (n = 5)	57 ± 17 (n = 3)
$DmNa_v1^{rNav1.2a(DIV/S3-MFLA)}$	495 ± 113 (n = 3)	1.4 ± 0.1 (n = 3)
$DmNa_v1^{rNav1.2a(DI/S5-SS1)}$	>2500 (n = 3)	0.65 ± 0.1 (n = 3)
$DmNa_v1^{rNav1.2a(DI/SS2-S6)}$	>5000 (n = 3)	0.54 ± 0.06 (n = 2)
$DmNa_v1^{rNav1.2a(D1/S5-SS1+SS2-S6)}$	123 ± 26 (n = 3)	0.48 ± 0.12 (n = 3)
$DmNa_v1^{rNav1.2a(site-3\ face)a}$	26.7 ± 3.1 (n = 5)	241 ± 47 (n = 4)
$DmNa_v1^{rNav1.2a(site-3\ face-E1613D)}$	22.5 ± 1.9 (n = 3)	0.37 ± 0.03 (n = 4)
$rNa_v1.2a^{E1613D}$	14.5 ± 5.7 (n = 4)	18.8 ± 3.3 (n = 4)
$rNa_v1.2a$ unmodified	13.6 ± 1.4 (n = 3)	17,800 ± 357 (n = 5)

[a] Site-3 face denotes DI/S5-SS1+SS2-S6, DIV/S1-S2+S3-S4 exchanged in $DmNa_v1$ by their $rNa_v1.2a$ equivalents.

and $DmNa_v1^{rNav1.2(DI/SS2-S6)}$ to Lqh2 was as poor as that of $DmNa_v1$, and the LqhαIT effect on these channel chimeras hardly changed (Table 1). Thus, single loop substitutions were not very effective suggesting that there may be a cooperative effect of the two extracellular loops in the pore module on the ability of Lqh2 to interact with the brain sodium channel. Overall, these results indicated that both the gating module of DIV and the pore module of DI were required to form a complete Lqh2 receptor site in $DmNa_v1$.

Substitution of Residues in DIV External Loop That Differ between $rNa_v1.2a$ and $DmNa_v1$—The substantial role of DIV/S3-S4 in channel sensitivity to the two α-toxins (Table 1) as well as previous reports on changes in activity of α-toxins upon substitution of Glu-1613 in $rNa_v1.2a$ (21) and its Asp-1428 and Asp-1701 equivalents in $rNa_v1.4$ (23, 33) and $DmNa_v1$ (7) suggested that differences in this loop between the two channels might be involved with the varying potency of α-toxins. Hence, we examined the effect of reciprocal exchange of Glu-1613 at $rNa_v1.2a$ and Asp-1701 at $DmNa_v1$ on channel sensitivity to Lqh2 and LqhαIT. Whereas the substitution D1701E at $DmNa_v1$ markedly reduced LqhαIT activity (139-fold decrease; Table 1), this channel mutant remained insensitive to Lqh2. In sharp contrast was the effect of the reciprocal substitution in $rNa_v1.2a$ (E1613D), which improved LqhαIT affinity by ~1000-fold, closely resembling the potency of Lqh2 at $rNa_v1.2a$ (EC_{50} = 18.8 ± 3.3 nM; Table 1; Fig. 3*B*). Following this striking result, we analyzed the Glu-to-Asp substitution in the context of the chimera $DmNa_v1^{rNav1.2a(site-3\ face)}$. We found that the activity of LqhαIT on $DmNa_v1^{rNav1.2a(site-3\ face-E1613D)}$ was restored (EC_{50} = 0.37 ± 0.03 nM) and was similar to the activity of the toxin at $DmNa_v1$, whereas Lqh2 activity persisted (Table 1; Fig. 3*A*). Thus, Glu-1613 at DIV/S3-S4 is a key factor that hinders LqhαIT interaction with receptor site-3 of the rat brain channel $rNa_v1.2a$.

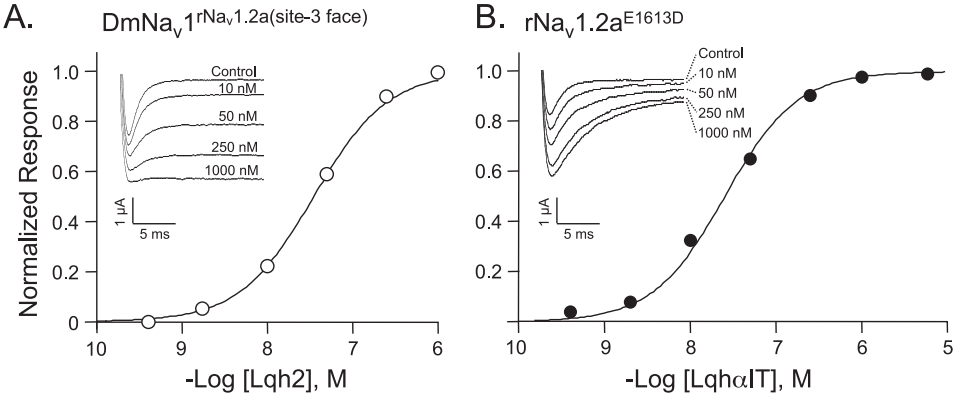

FIGURE 3. **Lqh2 and LqhαIT activities on modified channels.** *A*, dose response curve of Lqh2 on the channel chimera DmNa$_v$1$^{rNav1.2a(site\text{-}3\ face)}$ expressed in *Xenopus* oocytes. Each point represents mean ± S.E. of at least $n = 3$. *Inset*, representative traces of Lqh2 activity on the channel chimera. The oocytes were clamped at −80 mV, and currents were elicited by 50 ms depolarization to −20 mV from a −80 mV holding potential in the presence of increasing toxin concentrations. At each toxin concentration, the currents were allowed to reach a steady-state level prior to the final measurement (see "Experimental Procedures"). *B*, dose response curve of LqhαIT activity on the channel mutant rNa$_v$1.2a^{E1613D}. *Inset*, representative traces of LqhαIT activity on the channel mutant expressed in *Xenopus* oocytes using a similar protocol as described in *A*. A further increase in toxin concentration did not yield further inhibition of channel inactivation.

A prominent difference in this channel region is the amino acid composition of the distal part of DIV/S3 (positions 1697–1700 in DmNa$_v$1; Leu-Val-Leu-Ser *versus* positions 1609–1612 in rNa$_v$1.2a; Met-Phe-Leu-Ala; Fig. 1). Substitution of this amino acid stretch by its rNa$_v$1.2a equivalent resulted in a channel mutant, DmNa$_v$1$^{rNav1.2a(DIV/S3\text{-}MFLA)}$, whose sensitivity to Lqh2 increased 14-fold, with only a minor effect in its sensitivity to LqhαIT (Table 1), compared with DmNa$_v$1. This suggested that this region in DIV gating module of rNa$_v$1.2a plays a role in Lqh2 interaction with its receptor.

*Analysis of Voltage-dependent Dissociation of Lqh2 Mutants from Na$_v$1.2a*—The swap of the Lqh2 receptor at rNa$_v$1.2a onto DmNa$_v$1 indicated an important role of the gating module of DIV and pore module of DI in toxin recognition. On the toxin side, the bioactive surface of Lqh2 has recently been shown to be composed of two domains: the core domain (Phe-15, Arg-18, Trp-38, and Asn-44) and the NC domain (Lys-2, Thr-57, Lys-58; Fig. 2*A*; Ref. 29). On these grounds and the fact that binding of scorpion α-toxins is voltage-dependent (1, 34–37), which suggests toxin binding at the mobile voltage-sensing region, we analyzed which of the toxin bioactive domains interacts with the DIV gating module of rNa$_v$1.2a. This analysis was based on the assumption that the dissociation of toxin mutants upon depolarization would vary from that of the unmodified toxin if the substitutions affect a site of interaction with the channel gating module.

We first analyzed the voltage-dependent dissociation of Lqh2 at a saturating concentration from rNa$_v$1.2a expressed in *Xenopus* oocytes by applying a series of depolarizing prepulses to +105 mV of variable durations (see "Experimental Procedures"). However, under this protocol with prepulse duration of up to 200 ms, the toxin had barely dissociated, as indicated by the persistent inhibition of inactivation following the test pulse (Fig. 4*A*). Considerable dissociation of Lqh2 was obtained following a prepulse duration of at least 500 ms, and the apparent toxin effect was nearly abolished after 2 s (not shown). Because depolarizing prepulses exceeding 200 ms promote channel entrance into slow inactivation (38), we limited the assays with saturating toxin concentrations to a 200-ms depolarizing prepulse (Fig. 4*A*, *inset*). The same protocol was used to analyze Lqh2 mutants K2A, F15A, N44A, and T57A. This analysis revealed that the voltage-dependent dissociation of Lqh2 substituted at the core domain was markedly enhanced, especially for F15A and N44A. The $V_{½}$ for dissociation of mutants Lqh2^{F15A} and Lqh2^{N44A} was 82.5 ± 0.6 and 53 ± 2.7 mV, respectively, compared with 129 ± 13 mV for Lqh2 (Table 2), and a complete dissociation was observed following a depolarizing prepulse to +105 mV (Fig. 4*A*). On the other hand, the voltage-dependent dissociation of toxin mutants Lqh2^{K2A} and Lqh2^{T57A} of the NC domain (Fig. 2; Ref. 29) was similar to that of the unmodified toxin, despite a large increase in their EC_{50} values (Fig. 4*B* and Table 2). These results have suggested that the core domain of Lqh2 interacts with a channel region undergoing modification upon depolarization.

Effects of Channel Substitutions on Voltage-dependent Dissociation of Lqh2—Because an E1613R substitution in rNa$_v$1.2a has been shown to enhance the dissociation of the α-toxin Lqq5 (21), we examined the effects of charge neutralization and inversion at this position (E1613N and E1613R) on Lqh2 voltage-dependent dissociation (Tables 2 and 3). Notably, Lqh2 voltage-dependent dissociation off rNa$_v$1.2a^{E1613N} and rNa$_v$1.2a^{E1613R} channel mutants was markedly facilitated compared with its dissociation off the unmodified channel. The dissociation off rNa$_v$1.2a^{E1613R} was more prominent as it began at +40 mV and was complete following a prepulse to +105 mV (Fig. 4, *A* and *C*, and Table 2). However, despite the substantial shift in $V_{½}$ for both channel mutants, the EC_{50} values of Lqh2 barely changed (Tables 2 and 3). This result suggested that substitution of Glu-1613 at DIV/S3-S4 impairs an interaction of Lqh2 with an activated and/or fast-inactivated channel state.

Based on the results of the dissociation assays, we examined the effects of Lqh2 and its bioactive surface mutants on a number of channel mutants modified at the DIV extracellular loop S1–S2, the distal region of S3 and the beginning of S3–S4 (Table 3). These channel determinants were selected on the basis of the swap experiments, which suggested that they determine the selectivity of Lqh2, and on unpublished results of the effects of point mutations at DIV/S1-S2 on Lqh2 activity (39). Of all

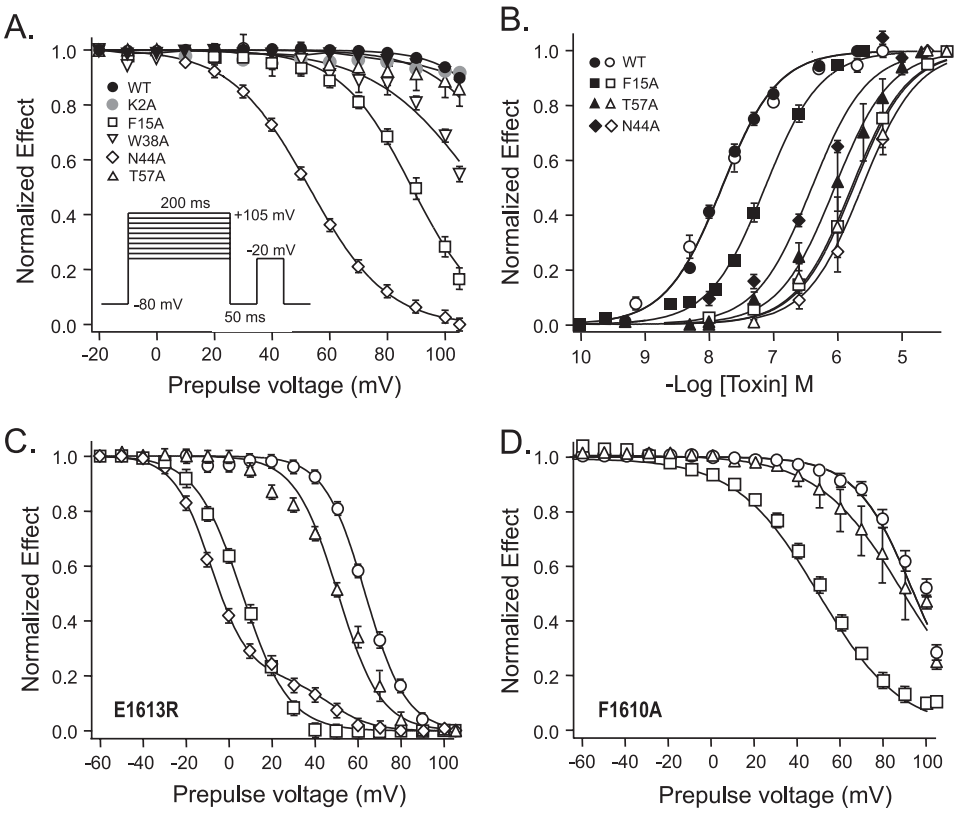

FIGURE 4. **Effects of substitutions in Lqh2 on activity and voltage-induced dissociation off rNa$_v$1.2a and its F1610A and E1613R mutants.** *A*, dissociation of Lqh2 and derivatives off rNa$_v$1.2a upon depolarizing prepulses. Toxin effect was monitored by a test pulse to −20 mV as a function of 200 ms varying depolarizing prepulses (between −20 and +105 mV; see *inset* and "Experimental Procedures"). Note the difference between core domain to NC domain toxin mutants. *B*, dose-dependent effect of Lqh2 mutants on rNa$_v$1.2a (*filled symbols*) and channel mutant rNa$_v$1.2a^{E1613R} (*open symbols*). *C*, dissociation of Lqh2 and derivatives off rNa$_v$1.2a^{E1613R} channel mutant upon depolarizing prepulses. *D*, dissociation of Lqh2 and derivatives off rNa$_v$1.2a^{F1610A} channel mutant upon depolarizing prepulses. Symbols in *C* and *D* are as described in *B*. The voltage protocol in *C* and *D* is identical to that described in *A*.

TABLE 2

Effects of Lqh2 mutants and their voltage-induced dissociation off rNa$_v$1.2a and the F1610A and E1613R channel mutants

The EC_{50} values for rNa$_v$1.2a are from Kahn *et al.* (29). The voltage at which 50% of the toxin dissociated ($V_{½}$) was calculated from the slopes presented at Fig. 4, *A*, *C*, and *D*. The values provided are mean ± S.E. of three to six measurements (*n*). ND, not determined (when the EC_{50} values could not be calculated because a saturating effect could not be reached).

	Toxin					
Channel	**WT**	**K2A**	**F15A**	**W38A**	**N44A**	**T57A**
rNa$_v$1.2a						
EC_{50} (nM)	13.6 ± 1.4	179 ± 22	72 ± 3.7	1180 ± 207	394 ± 43	1220 ± 40
$V_{½}$ (mV)	129 ± 13	>130	82.5 ± 0.6	111 ± 2	53 ± 2.7	>130
F1610A						
EC_{50} (nM)	63 ± 3.6	864 ± 39	2540 ± 160	3880 ± 76	ND	1820 ± 307
$V_{½}$ (mV)	93.8 ± 7.2	ND	49 ± 3.8	ND	ND	89 ± 6.4
E1613R						
EC_{50} (nM)	15.7 ± 1.6	ND	1640 ± 91	ND	3430 ± 234	1760 ± 203
$V_{½}$ (mV)	64.4 ± 4.4	ND	6.0 ± 0.3	ND	−10.7 ± 2[a]	50 ± 1.6

[a] N44A dissociation was best fit with a two-component Boltzmann distribution with a major component of 0.69, $V_{½}$ = −10.7 ± 2 mV, and a minor component, $V_{½}$ = 45 ± 1 mV.

channel mutants examined, prominent changes in Lqh2 EC_{50} values were obtained only for T1560A (DIV/S1-S2) and F1610A (distal region of DIV/S3; Tables 2 and 3).

Voltage-dependent Dissociation of Toxin Mutants from Channel Mutants—Analysis of the voltage-dependent dissociation of Lqh2 mutants Lqh2^{F15A} and Lqh2^{N44A} off rNa$_v$1.2a^{E1613R} revealed substantial enhancement, as indicated by the prominent shifts in $V_{½}$ to more negative membrane potentials ($V_{½}$ values of 6.0 ± 0.3 mV and −10.7 ± 2 mV, respectively, compared with 64.4 ± 4.4 mV for Lqh2; Fig. 4*C*; Table 2). In light of this result, we sought other residues that putatively interact with Lqh2. As replacement of the Leu-Val-Leu-Ser sequence at the C-terminal end of DIV/S3 in DmNa$_v$1 by its rNa$_v$1.2a equivalent, Met-Phe-Leu-Ala, resulted in gain of Lqh2 function at the chimeric channel, DmNa$_v$1$^{rNav1.2a(DIV/S3-MFLA)}$ (Table 1), we examined the effect of substitutions M1609A and F1610A at rNa$_v$1.2a on Lqh2 activity. Whereas substitution M1609A had no effect (Table 3), the substitution F1610A resulted in 5-fold increase in the EC_{50} of Lqh2 (Table 2). Accordingly, we analyzed the effect of F1610A substitution

on the voltage-dependent dissociation of Lqh2 and its mutant derivatives. As shown in Fig. 4*D* and Table 2, the dissociation of Lqh2 off $rNa_v1.2a^{F1610A}$ was markedly facilitated and observed at a lower membrane potential compared with the toxin dissociation off the unmodified channel. Furthermore, whereas the dissociation of the NC-domain toxin mutant, $Lqh2^{T57A}$, off $rNa_v1.2a^{F1610A}$ resembled that of the unmodified toxin, the dissociation of the core domain toxin mutant $Lqh2^{F15A}$ off $rNa_v1.2a^{F1610A}$ was markedly facilitated (Fig. 4*D*; Table 2). These results suggested that upon interaction, the core domain of Lqh2 is in close proximity to the distal region of S3 at DIV in the rat brain sodium channel.

TABLE 3

Lqh2 activity and voltage-dependent dissociation off $rNa_v1.2a$ and mutants

Determination of the dose-dependent effect of the toxin (removal of fast inactivation) is described in detail under "Experimental Procedures", and the EC_{50} values provided are mean ± S.E. of at least three measurements (*n*). $V_{½}$, the voltage at which 50% of the toxin dissociated off the channel.

Channel	Toxin (Lqh2)	
	EC_{50}	$V_{½}$
	nM	*mV*
$rNa_v1.2a$	13.6 ± 1.4	129 ± 13
T1560A	55 ± 4.2	>105
M1609A	22 ± 2.9	>105
L1611A	12.8 ± 1.8	>105
E1613N	11.4 ± 1.8	101 ± 1.7
Y1618A	16.3 ± 2.2	>105
F1619A	17.4 ± 1.7	>105
V1620A	14.2 ± 0.9	>105

DISCUSSION

Determination of receptor sites of Na_v modifiers is complex due to the lack of channel structure and their conformational rearrangements during gating. The experimental approach in the present study was to first identify channel regions involved in toxin selectivity and then dissect the relevant regions in search for specific residues associated with the receptor site. Although receptor site-3 is not necessarily constituted from components that differ between the brain and insect sodium channels, the successful swap and gain of high activity of Lqh2 at the chimeric channel $DmNa_v1^{rNav1.2a(site\text{-}3\ face)}$ has indicated that the external loops of the gating module of domain IV and pore module of domain I in $rNa_v1.2a$ play an important role in toxin selectivity and that they are spatially arranged in the chimeric channel as in $rNa_v1.2a$. The inverse experiment to construct $rNa_v1.2a$ such that it acquires high sensitivity to LqhαIT surprisingly did not require swap of external loops from $DmNa_v1$. Instead, a single conservative substitution, E1613D, converted the brain channel to high sensitivity toward LqhαIT. In the skeletal muscle channel $Na_v1.4$ and cardiac channel $Na_v1.5$, the position equivalent to Glu-1613 is occupied by an Asp residue, and both channels are sensitive to LqhαIT (32, 36). Moreover, substitution at this position in $rNa_v1.4$ (D1428E) decreased the effect of LqhαIT (23). These observations are in concert with the gain of function of LqhαIT at the E1613D mutant of $rNa_v1.2a$ and indicate that Glu-1613 at DIV/S3-S4 of $rNa_v1.2a$ is in close proximity to the surface of interaction with

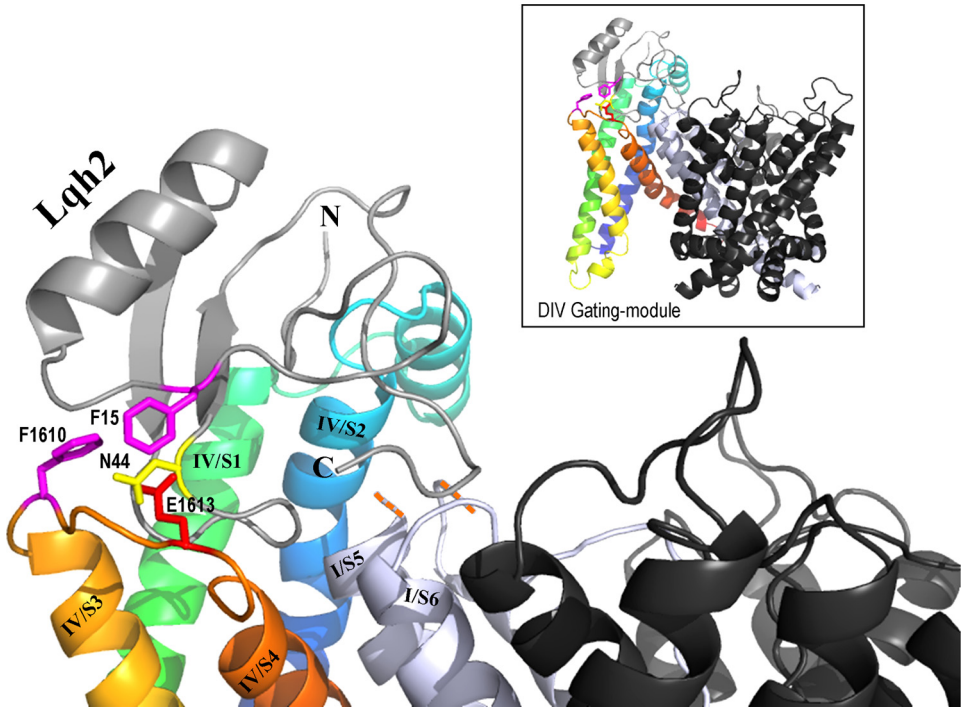

FIGURE 5. **Model of Lqh2 interaction with $rNa_v1.2$ resting state.** The external loops DIV/S1-S2 and S3-S4 of $rNa_v1.2a$ were constructed on the structural model of $K_v1.2$ in its resting state (43) using the Swiss-PdbViewer. The internal loops and the gating modules of DI, DII, and DIII were removed. Shown in *black* are the remaining pore modules of DII, DIII, and DIV, whereas the DI pore module is shown in *light gray*. Due to the substantial difference in size, the DI/S5-SS1 external loop is omitted (indicated by the *orange dashes*). DIV/S1 is shown in *green*, DIV/S2 is shown in *blue*, DIV/S3 is shown in *light orange*, and DIV/S4 is shown in *dark orange*. Lqh2 modeling relied on its close resemblance to Aah2 (29; Protein Data Bank code 1AHO). Phe-15 and Asn-44 are bioactive residues of Lqh2 that are in close proximity to Phe-1610 and Glu-1613 of the channel, respectively (colored sticks according to their chemical nature). Docking of Lqh2 core domain at DIV gating module was performed using DockingServer. Although the residues of the toxin NC domain that may interact with residues at DI/S5-SS1 and DIV/S1-S2 have not been clarified yet, further modeling was performed manually to show this proximity, while avoiding side chain clashes. The final figure was drawn using PyMOL.

LqhαIT. The gain of $rNa_v1.2a$ sensitivity to LqhαIT upon a single substitution demonstrates that the brain channel bears a receptor site for LqhαIT, and the primary reason for lack of LqhαIT activity is the hindrance caused by Glu-1613. Furthermore, these results also suggest that receptor sites 3 at both the brain and insect channels are similar although not identical.

The interaction of DIV/S3-S4 external loop with scorpion α-toxins has been demonstrated in previous studies (21, 23, 40, 41), and it was proposed that the positively charged S4 segment moves outwards upon depolarization and is capable of removing the bound toxin from its receptor site (1, 5, 15, 16, 21, 34). Perturbation of this movement by the bound toxin then inhibits the subsequent conformational change required for fast inactivation. However, in contrast to the large detrimental effect of E1613R substitution at $rNa_v1.2a$ on Lqq5 activity (21), this substitution had comparatively little effect on Lqh2 activity except when assayed in the toxin dissociation protocol (Fig. 4*A*; Table 2). This difference in effect may be attributed to the difference between the toxins but also to the experimental system employed for channel expression, such that DIV/S3-S4 may not be displayed identically when expressed in mammalian cells *versus Xenopus* oocytes. Indeed, we find a large effect of the E1613R mutation on Lqh2 action for $Na_v1.2$ channels expressed in the human embryonic kidney cell line tsA-201 (39). Nevertheless, the results obtained with Lqq5 and Lqh2 applied onto $rNa_v1.2a$ expressed in mammalian cells (21, 23, 39) and the results regarding toxin dissociation obtained in this study corroborate the suggestion that Glu-1613 in $rNa_v1.2a$ is in very close proximity to the interacting surface of scorpion α-toxins with this brain sodium channel.

On the basis of the bipartite bioactive surface of Lqh2 (29) and the successful swap of its receptor, we assume that Lqh2 interacts with the channel such that one of the two functional domains at the toxin surface recognizes the gating module at DIV and the other toxin domain interacts with the pore module of DI. The involvement of the distal part of DIV/S3 in this interaction might take place within a crevice in the membrane-channel interface that enables access of the toxin core domain, a scenario that resembles the interaction of a scorpion β-toxin with DII of $rNa_v1.2a$ (42).

Our suggestion that the core domain of Lqh2 interacts with DIV gating module is based on the findings of large changes in the depolarization-induced dissociation of the core domain toxin mutants compared with the unmodified toxin (Fig. 4*A*), as well as on the enhanced dissociation of Lqh2 from the channel mutants modified at this channel region, $rNa_v1.2a^{E1613R}$ and $rNa_v1.2a^{F1610A}$ (Table 2; Fig. 4, *C* and *D*). We used these data to construct an initial model of the putative interaction of Lqh2 with $rNa_v1.2a$ by employing the three-dimensional structure of the potassium channel $K_v1.2$ (43) and assuming that the intersegmental region of both channel types would be similar (Fig. 5). In this initial model, Phe-15 of the toxin is in close proximity to Phe-1610 in DIV/S3 and to Glu-1613 in DIV/S3-S4, whereas Asn-44 of the toxin is in close proximity to Glu-1613, in agreement with our conclusion that the toxin core domain interacts with the voltage-sensing module of the channel. Although at this stage we are unable to determine which of the toxin domains interacts first with the channel, from the toxin unbinding experiments it seems that, upon depolarization, dissociation of the toxin off the channel is initiated at the core domain.

In summary, this study reveals sodium channel determinants involved in scorpion α-toxin selectivity as well as illuminates for the first time the α-toxin domain that interacts with the channel voltage sensor, which enables initial modeling of its docking at the channel. Further mutagenesis and double-mutant cycle analysis, including residues that are spatially conserved in sodium channels, are required to identify the individual amino acid residues in the DI/S5-S6 and DIV/S1-S2 loops that participate in toxin binding.

REFERENCES

1. Catterall, W. A. (2000) *Neuron* **26,** 13–25
2. Zlotkin, E. (1999) *Annu. Rev. Entomol* **44,** 429–455
3. Gordon, D., Karbat, I., Ilan, N., Cohen, L., Kahn, R., Gilles, N., Dong, K., Stühmer, W., Tytgat, J., and Gurevitz, M. (2007) *Toxicon* **49,** 452–472
4. Cestèle, S., and Catterall, W. A. (2000) *Biochimie* **82,** 883–892
5. Ulbricht, W. (2005) *Physiol. Rev.* **85,** 1271–1301
6. Gilles, N., Harrison, G., Karbat, I., Gurevitz, M., Nicholson, G. M., and Gordon, D. (2002) *Eur. J. Biochem.* **269,** 1500–1510
7. Moran, Y., Kahn, R., Cohen, L., Gur, M., Karbat, I., Gordon, D., and Gurevitz, M. (2007) *Biochem. J.* **406,** 41–48
8. Feng, G., Deák, P., Chopra, M., and Hall, L. M. (1995) *Cell* **82,** 1001–1011
9. Warmke, J. W., Reenan, R. A., Wang, P., Qian, S., Arena, J. P., Wang, J., Wunderler, D., Liu, K., Kaczorowski, G. J., Van der Ploeg, L. H., Ganetzky, B., and Cohen, C. J. (1997) *J. Gen. Physiol.* **110,** 119–133
10. Qu, Y., Curtis, R., Lawson, D., Gilbride, K., Ge, P., DiStefano, P. S., Silos-Santiago, I., Catterall, W. A., and Scheuer, T. (2001) *Mol. Cell Neurosci.* **18,** 570–580
11. Yu, F. H., Westenbroek, R. E., Silos-Santiago, I., McCormick, K. A., Lawson, D., Ge, P., Ferriera, H., Lilly, J., DiStefano, P. S., Catterall, W. A., Scheuer, T., and Curtis, R. (2003) *J. Neurosci.* **23,** 7577–7585
12. Derst, C., Walther, C., Veh, R. W., Wicher, D., and Heinemann, S. H. (2006) *Biochem. Biophys. Res. Commun.* **339,** 939–948
13. Tombola, F., Pathak, M. M., and Isacoff, E. Y. (2006) *Annu. Rev. Cell Dev. Biol.* **22,** 23–52
14. West, J. W., Patton, D. E., Scheuer, T., Wang, Y., Goldin, A. L., and Catterall, W. A. (1992) *Proc. Natl. Acad. Sci. U.S.A.* **89,** 10910–10914
15. Yang, Y. C., and Kuo, C. C. (2003) *J. Neurosci.* **23,** 4922–4930
16. Goldin, A. L. (2003) *Curr. Opin. Neurobiol.* **13,** 284–290
17. Sheets, M. F., Kyle, J. W., Kallen, R. G., and Hanck, D. A. (1999) *Biophys. J.* **77,** 747–757
18. Campos, F. V., Chanda, B., Beirão, P. S., and Bezanilla, F. (2008) *J. Gen. Physiol.* **132,** 251–263
19. Thomsen, W. J., and Catterall, W. A. (1989) *Proc. Natl. Acad. Sci. U.S.A.* **86,** 10161–10165
20. Tejedor, F. J., and Catterall, W. A. (1990) *Cell Mol. Neurobiol.* **10,** 257–265
21. Rogers, J. C., Qu, Y., Tanada, T. N., Scheuer, T., and Catterall, W. A. (1996) *J. Biol. Chem.* **271,** 15950–15962
22. Qu, Y., Rogers, J. C., Chen, S. F., McCormick, K. A., Scheuer, T., and Catterall, W. A. (1999) *J. Biol. Chem.* **274,** 32647–32654
23. Leipold, E., Lu, S., Gordon, D., Hansel, A., and Heinemann, S. H. (2004) *Mol. Pharmacol.* **65,** 685–691
24. Leipold, E., Hansel, A., Olivera, B. M., Terlau, H., and Heinemann, S. H. (2005) *FEBS Lett.* **579,** 3881–3884
25. Weinberger, H., Moran, Y., Gordon, D., Turkov, M., Kahn, R., and Gurevitz, M. (2010) *Mol. Biol. Evol.* **27,** 1025–1034
26. Karbat, I., Frolow, F., Froy, O., Gilles, N., Cohen, L., Turkov, M., Gordon, D., and Gurevitz, M. (2004) *J. Biol. Chem.* **279,** 31679–31686
27. Karbat, I., Kahn, R., Cohen, L., Ilan, N., Gilles, N., Corzo, G., Froy, O., Gur, M., Albrecht, G., Heinemann, S. H., Gordon, D., and Gurevitz, M. (2007) *FEBS J.* **274,** 1918–1931
28. Liu, L. H., Bosmans, F., Maertens, C., Zhu, R. H., Wang, D. C., and Tytgat,

J. (2005) *FASEB J.* **19,** 594–596
29. Kahn, R., Karbat, I., Ilan, N., Cohen, L., Sokolov, S., Catterall, W. A., Gordon, D., and Gurevitz, M. (2009) *J. Biol. Chem.* **284,** 20684–20691
30. Shichor, I., Zlotkin, E., Ilan, N., Chikashvili, D., Stuhmer, W., Gordon, D., and Lotan, I. (2002) *J. Neurosci.* **22,** 4364–4371
31. Wallner, M., Weigl, L., Meera, P., and Lotan, I. (1993) *FEBS Lett.* **336,** 535–539
32. Chen, H., and Heinemann, S. H. (2001) *J. Gen. Physiol.* **117,** 505–518
33. Gordon, D., Kallen, R. G., and Heinemann, S. H. (2004) in *Neurotox '03: Neurotoxicological Targets from Functional Genomics & Proteomics* (Beadle, D., Mellor, I. R., and Usherwood, P. N., eds) pp. 59–68, Society of Chemical Industry, London
34. Catterall, W. A. (1979) *J. Gen. Physiol.* **74,** 375–391
35. Strichartz, G. R., and Wang, G. K. (1986) *J. Gen. Physiol.* **88,** 413–435
36. Chen, H., Gordon, D., and Heinemann, S. H. (2000) *Pflugers Arch.* **439,** 423–432
37. Gilles, N., Leipold, E., Chen, H., Heinemann, S. H., and Gordon, D. (2001) *Biochemistry* **40,** 14576–14584
38. Featherstone, D. E., Richmond, J. E., and Ruben, P. C. (1996) *Biophys. J.* **71,** 3098–3109
39. Wang, J., Yarov-Yarovoy, V., Kahn, R., Gordon, D., Gurevitz, M., Scheuer, T., and Catterall, W. A. (2011) *Biophys. J.* **100,** 422a
40. Schnur, E., Turkov, M., Kahn, R., Gordon, D., Gurevitz, M., and Anglister, J. (2008) *Biochemistry* **47,** 911–921
41. Bosmans, F., Martin-Eauclaire, M. F., and Swartz, K. J. (2008) *Nature* **456,** 202–208
42. Cestèle, S., Yarov-Yarovoy, V., Qu, Y., Sampieri, F., Scheuer, T., and Catterall, W. A. (2006) *J. Biol. Chem.* **281,** 21332–21344
43. Pathak, M. M., Yarov-Yarovoy, V., Agarwal, G., Roux, B., Barth, P., Kohout, S., Tombola, F., and Isacoff, E. Y. (2007) *Neuron* **56,** 124–140